Electronic structure and spectroscopy of luminescent heterobimetallic Pt(II)–Rh(I), Au(I)–Rh(I), and Ag(I)–Rh(I) complexes

ARTICLE *in* INORGANIC CHEMISTRY · AUGUST 1993

Impact Factor: 4.76 · DOI: 10.1021/ic00068a006

4 AUTHORS, INCLUDING:

Yu Wang
National Taiwan University
440 PUBLICATIONS **6,225** CITATIONS

SEE PROFILE

Electronic Structure and Spectroscopy of Luminescent Heterobimetallic Pt(II)-Rh(I), Au(I)-Rh(I), and Ag(I)-Rh(I) Complexes

Hon-Kay Yip,[†] Hsiu-Mei Lin,[‡] Yu Wang,[‡] and Chi-Ming Che*[,†,‡]

Departments of Chemistry, The University of Hong Kong, Pokfulam Road, Hong Kong, and National Taiwan University, Taipei, Taiwan

Received October 28, 1992

The spectroscopic and luminescent properties of the heterobimetallic $[PtRh(dppm)_2(CN)_2(CN\text{-}t\text{-}Bu)_2]ClO_4$, $[AuRh(dppm)_2(CN\text{-}t\text{-}Bu)_2](ClO_4)_2$, and $[AgRh(dppm)_2(CN\text{-}t\text{-}Bu)_2](ClO_4)_2$ complexes were investigated. All the three complexes display an intense $^1(d\sigma^* \rightarrow p\sigma)$ transition at 473 nm ($\epsilon_{max} = 1.34 \times 10^4$ M^{-1} cm^{-1}), 455 nm ($\epsilon_{max} = 2.40 \times 10^4$ M^{-1} cm^{-1}), and 425 nm ($\epsilon_{max} = 1.68 \times 10^4$ M^{-1} cm^{-1}), respectively. A molecular orbital calculation on the model complex $[PtRh(dmpm)_2(CN)_2(CN\text{-}t\text{-}Bu)_2]^+$ (dmpm = bis(dimethylphosphino)methane) suggests that the $d\sigma^*$ orbital is mainly derived from the $4d_{z^2}$ of Rh and the $p\sigma$ is made up of π^* of isocyanide and $5p_z$ of Rh. In each case, the $^1(d\sigma^* \rightarrow p\sigma)$ transition has substantial Rh $\rightarrow \pi^*$(isocyanide, phosphine) charge-transfer character. Excitation of solid samples of the complexes leads to phosphorescence derived from the $^3(d\sigma^* p\sigma)$ excited state.

Introduction

The spectroscopy and photochemistry of heterobimetallic complexes have recieved much attention recently. Systems studied include various combinations of different metal ions such as d^{10}-main group ions (Au-Pb, Au-Tl[1a]), d^8-main group ions (Pt-Tl,[1b] Ir-Tl,[1c] Ir-Pb[1d]), and d^{10}-d^8 systems (Au-Pt,[1e] Au-Ir[1f,g]). Our recent work on the d^{10}-d^8 $[Au^IPt^{II}(dppm)_2(CN)_2]^+$ [1e] (dppm = bis(diphenylphosphino)methane) demonstrated that apart from the well-established homodinuclear d^8-d^8 complexes, heterobimetallic complexes are also very promising systems for photochemical studies. To further our study in metal-metal interaction and photophysics of heterobimetallic complexes, we examine the spectroscopic and photophysical properties of luminescent dinuclear complexes $[Pt^{II}Rh^I(dppm)_2(CN)_2(CN\text{-}t\text{-}Bu)_2]ClO_4$ and $[MRh(dppm)_2(CN\text{-}t\text{-}Bu)_2](ClO_4)_2$ (M = Au^+, Ag^+). The complexes are of special interest since they bears similar structure of the well-established d^8-d^8 dimers such as $[Pt_2(P_2O_5H_2)_4]^{4-}$ [2] and $[Rh_2(1,3\text{-diisocyanopropane})_4]^{2+}$ [3] and d^{10}-d^{10} dimers such as $[Au_2(dppm)_2]^{2+}$.[4] Since the completion of our work, Balch and co-workers reported the spectroscopic properties and X-ray crystal structure of $[Pt^{II}Rh^I(dppm)_2(CN)_2(CN\text{-}t\text{-}Bu)_2]^+$.[5]

Experimental Section

Materials. $[PtRh(dppm)_2(CN)_2(CO)Cl]$,[5a] $[MRh(dppm)_2(CN\text{-}t\text{-}Bu)_2](ClO_4)_2$ (M = Au^+, Ag^+),[5b] and *trans*-$[Rh(PPh_3)_2(CO)Cl]$[5c] were prepared by the literature methods.

Synthesis of $[PtRh(dppm)_2(CN)_2(CN\text{-}t\text{-}Bu)_2]ClO_4$. *tert*-Butyl isocyanide (CN-*t*-Bu) (0.028 g, 0.34 mmol) was added to a methanol suspension of $[Pt^{II}Rh^I(dppm)_2(CN)_2(CO)(Cl)]$ (0.2 g, 0.17 mmol), and the mixture was stirred at room temperature. Efflorescence was observed upon addition, and the solution was stirred until a clear orange solution was obtained. The solution was then filtered, and an orange precipitate was obtained after adding $LiClO_4$ to the filtrate. The orange solid was recrystallized by diffusing diethyl ether into acetonitrile. Yield = 89%. Needlelike crystals obtained by this method were further used for X-ray crystallographic study. IR: 2130 cm^{-1} (ν(C≡N) of cyanide); 2145 cm^{-1} (ν(C≡N) of isocyanide). ^1H NMR: δ (ppm) = 0.769 (s, 18H, methyl protons of the isocyanides), 4.32 (m, 4H, methylene protons of dppm), and 7.37, 7.80 (m, 40H, phenyl protons of dppm). ^{31}P NMR data: δ (ppm) = 19.11 (d, *P*-Rh-*P*, ^1J(Rh-P) = 105 Hz), 2.47 (pseudotriplet, *P*-Pt-*P*, ^1J(Pt-P) = 2460 Hz). The structure of the complex was established by X-ray crystal analysis.[7]

Synthesis of *trans*-$[Rh(PPh_3)_2(CN\text{-}t\text{-}Bu)_2]ClO_4$. To a methanol suspension of *trans*-$[Rh(PPh_3)_2(CO)Cl]$ (0.2 g, 0.29 mmol) was added *tert*-butyl isocyanide (0.048 g, 0.58 mmol). A clear solution immediately resulted. The solution was filtered, and a yellow solid was obtained after adding $LiClO_4$ to the filtrate. The product was recrystallized by slow diffusion of diethyl ether into an acetonitrile solution. Yield = 75%. IR: 2105 cm^{-1} (s, sh) (ν(C≡N). ^1H NMR: δ (ppm) = 0.61 (s, 18H, methyl protons of *tert*-butyl isocyanide), 7.2-7.8 (m, 40H, phenyl protons of PPh_3). Anal. Calcd for $RhC_{46}H_{48}N_2P_2ClO_4$: C, 61.8; H, 5.4; N, 3.1. Found: C, 61.4; H, 5.2; N, 3.0.

Instrumentation. Electronic absorption spectra were recorded on a Milton Roy Spectronic 3000 array spectrometer. Room-temperature and 77 K emission spectra were recorded on a Spex 1681 spectrofluorometer. Emission lifetimes were measured by using a Spectra-Physics DCR-3 Nd:YAG pulsed laser with signal acquired by a Tektronix 2430 digitial analyzer. ^{31}P and ^1H NMR spectra were recorded on a 270-MHz Jeol JMN-GSX 270 spectrometer. The ^{31}P chemical shifts were reported relative to H_3PO_4.

Molecular Orbital Calculations. EHMO calculations were carried out using the geometric parameters from the X-ray diffraction data.[7] The basis functions of Pt and Rh were taken from the literature.[8] Molecular orbital calculations were made with the ICON program.[9] For the wave function plots, the MOPLOT program and a locally developed contour plot routine were used.[10]

† The University of Hong Kong.
‡ National Taiwan University.

(1) (a) Wang, S.; Garz'on, G.; King, C.; Wang, J.-C.; Fackler, J. P., Jr. *Inorg. Chem.* **1989**, *28*, 4623. (b) Nagle, J. K.; Balch, A. L.; Olmstead, M. M. *J. Am. Chem. Soc.* **1988**, *110*, 319. (c) Balch, A. L.; Neve, F.; Olmstead, M. M. *J. Am. Chem. Soc.* **1991**, *113*, 2995. (d) Balch, A. L.; Catalano, V. J.; Chatfield, M. A.; Nagle, J. K.; Olmstead, M. M.; Reedy, P. E. *J. Am. Chem. Soc.* **1991**, *113*, 1252. (e) Yip, H.-K.; Che, C.-M.; Peng, S.-M. *J. Chem. Soc., Chem. Commun.* **1991**, 1626. (f) Balch, A. L.; Catalano, V. J.; Olmstead, M. M. *Inorg. Chem.* **1990**, *29*, 585. (g) Balch, A. L.; Catalano, V. J.; Noll, B. C.; Olmstead, M. M. *J. Am. Chem. Soc.* **1990**, *112*, 7558.
(2) Roundhill, D. M.; Gray, H. B.; Che, C.-M. *Acc. Chem. Res.* **1989**, *22*, 55.
(3) Mann, K. R.; Thich, J. A.; Bell, R. A.; Coyle, C. L.; Gray, H. B. *Inorg. Chem.* **1980**, *19*, 2462.
(4) (a) King, C.; Wang, J.-C.; Khan, N. I. Md.; Fackler, J. P. *Inorg. Chem.* **1989**, *28*, 2145. (b) Che, C.-M.; Kwong, H.-L.; Poon, C.-K.; Yam, V. W.-W. *J. Chem. Soc., Dalton Trans.* **1990**, 3215.
(5) Balch, A. L.; Catalano, V. J. *Inorg. Chem.* **1992**, *31*, 3934.
(6) (a) Hassan, F. S. M.; Markham, D. P.; Pringle, P. G.; Shaw, B. L. *J. Chem. Soc., Dalton Trans.* **1985**, 279. (b) Langrick, C. R.; Shaw, B. L. *J. Chem. Soc., Dalton Trans.* **1985**, 511. (c) Osborn, J. A.; Wilkinson, G. *Inorg. Synth.* **1990**, *28*, 77.
(7) Che, C.-M.; Wang, Y. Unpublished result.
(8) (a) Schilling, B. E. R.; Hoffmann, R. *J. Am. Chem. Soc.* **1979**, *101*, 3456. (b) Wheeler, R. A.; Piela, L.; Hoffmann, R. *J. Am. Chem. Soc.* **1988**, *110*, 7302.
(9) Both ICON and MOPLOT programs are from QCPE, Department of Chemistry, Indiana University, Bloomington, IN 47405.
(10) Tsai, C. J. Masters Thesis, National Taiwan University, 1982.

0020-1669/93/1332-3402$04.00/0

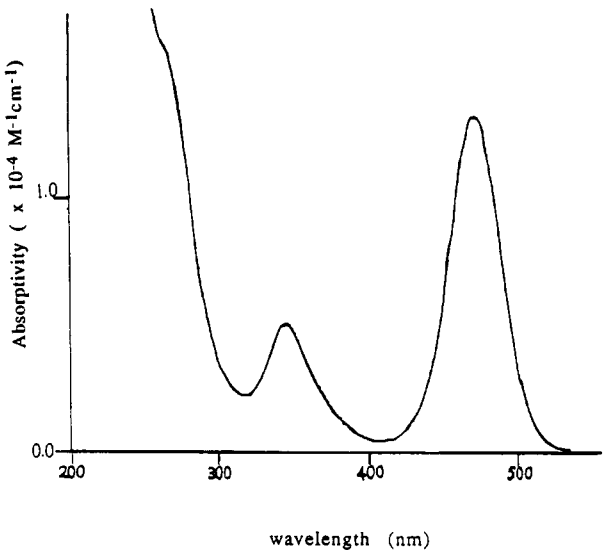

Figure 1. Absorption spectrum of an acetonitrile solution of $[Pt^{II}Rh^{I}(dppm)_2(CN)_2(CN\text{-}t\text{-}Bu)_2]ClO_4$ measured at room temperature.

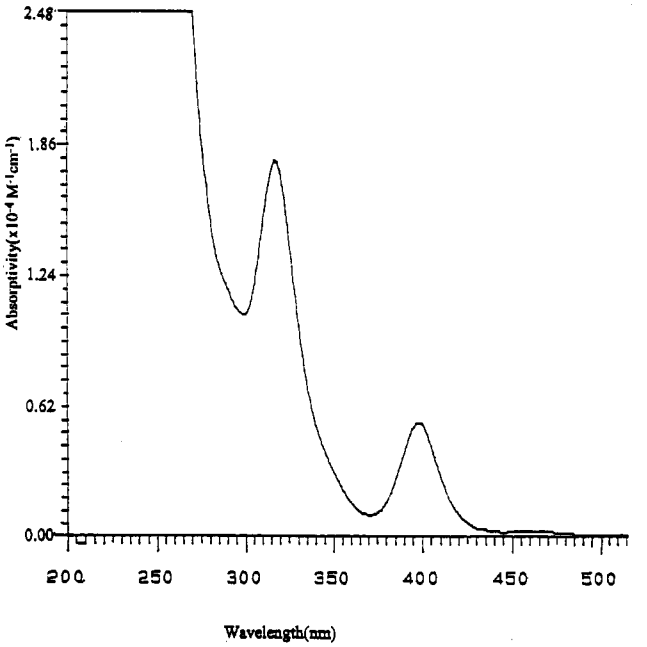

Figure 2. Absorption spectrum of *trans*-$[Rh^{I}(PPh_3)_2(CN\text{-}t\text{-}Bu)_2]^+$ measured in acetonitrile solution at room temperature.

Results and Discussion

Heterobimetallic d^8–d^8 Complex. The complex $[PtRh(dppm)_2(CN)_2(CN\text{-}t\text{-}Bu)_2]ClO_4$ has been characterized by X-ray crystallography.[7] It possesses essentially the same structure as the one reported by Balch,[5] being composed of two face-to-face square planar P–$Rh(CN\text{-}t\text{-}Bu)_2$–P and P–$Pt(CN)_2$–P units. The intramolecular Pt–Rh distance of 3.043(2) Å of the perchlorate complex[7] is slightly shorter than 3.079(1) Å found in the hexafluorophosphate complex.[5]

Figure 1 shows the absorption spectrum of an acetonitrile solution of $[Pt^{II}Rh^{I}(dppm)_2(CN)_2(CN\text{-}t\text{-}Bu)_2]ClO_4$ measured at room temperature. The spectrum is featured by an intense absorption band centered at 473 nm ($\epsilon_{max} = 1.34 \times 10^4\ M^{-1}\ cm^{-1}$) and a moderately intense absorption at 348 nm ($\epsilon_{max} = 5.09 \times 10^3\ M^{-1}\ cm^{-1}$). The 473-nm band has its shape and intensity similar to that of the $^1(d\sigma^* \rightarrow p\sigma)$ transition commonly found in dinuclear d^8–d^8 complexes such as $[Pt_2(P_2O_5H_2)]^{4-}$ [2] or $[Rh_2(1,3\text{-diisocyanopropane})_4]^{2+}$ [3] and is assigned to it accordingly. Interestingly, this band is situated in between the $^1(d\sigma^* \rightarrow p\sigma)$ transition energies of $[Pt_2(dppm)_2(CN)_4]$ (324 nm)[11] and $[Rh_2(dppm)_2(CN\text{-}t\text{-}Bu)_4]^{2+}$ (523 nm).[12] In order to understand the influence of the Pt(II) moiety on the $^1(d_{z^2} \rightarrow p_z, \pi^*)$ transition of *trans*-$[Rh(PR_3)_2(RNC)_2]^+$, the absorption spectrum of *trans*-$[Rh^{I}(PPh_3)_2(CN\text{-}t\text{-}Bu)_2]^+$ is examined. Figure 2 shows the absorption spectrum of *trans*-$[Rh^{I}(PPh_3)_2(CN\text{-}t\text{-}Bu)_2]^+$ measured in acetonitrile solution at room temperature. According to previous spectroscopic assignment of $[Rh(CNR)_4]$,[+13] the two intense absorption bands at 397 nm ($\epsilon_{max} = 5.50 \times 10^3\ M^{-1}\ cm^{-1}$) and 317 nm ($\epsilon_{max} = 1.81 \times 10^4\ M^{-1}\ cm^{-1}$) are assigned to the $^1(d_{z^2} \rightarrow p_z, \pi^*)$ and $^1(d_{xz,yz} \rightarrow p_z, \pi^*)$ transitions, respectively. The energy difference between the 473-nm band of $[Pt^{II}Rh^{I}(dppm)_2(CN)_2(CN\text{-}t\text{-}Bu)_2]^+$ and the $^1(d_{z^2} \rightarrow p_z, \pi^*)$ transition of *trans*-$[Rh^{I}(CN\text{-}t\text{-}Bu)_2(PPh_3)_2]^+$ is 4047 cm^{-1}. This value is small when it is compared with the related difference in energy between the $^1(d\sigma^* \rightarrow p\sigma)$ transition of homodinuclear d^8–d^8 complexes and the $^1(d_{z^2} \rightarrow p_z, \pi^*)$ transition of their monomeric counterparts (see Table I). From table I, it is clear that intramolecular metal–metal distance is one of the factors which determine the amount of energy difference between the transitions.[14] However, it is also obvious that, among all the six complexes listed in Table I, $[Pt^{II}Rh^{I}(dppm)_2(CN)_2(CN\text{-}t\text{-}Bu)_2]^+$ has the shortest metal–metal distance, but the energy difference of the transitions is the smallest. We attribute this to the difference in energy of the interacting d_{z^2} orbitals of Pt and Rh.

Table I. Energy Differences of $^1(d\sigma^* \rightarrow p\sigma)$ Transitions of Binuclear d^8–d^8 Complexes and $^1(d_{z^2} \rightarrow p_z)$ Transitions of Their Mononuclear Analogs

complex	energy diff between $^1(d\sigma^* \rightarrow p\sigma)$ and $^1(d_{z^2} \rightarrow p_z)$ transitions (cm^{-1})	metal–metal separation dists of binuclear complexes (Å)
$[Rh_2(dpam)_2(CO)_2(Cl)_2]$[a]	6500 [10]	3.396(1)[b]
$[Rh_2(TMB)_4]^{2+}$ [a]	7824 [3]	3.26 [3]
$[Ir_2(TMB)_4]^{2+}$	7641[c]	3.16(4)[c]
$[Pt_2(dppm)_2(CN)_4]$	5594 [7]	3.301(1) [7]
$[Rh_2(dppm)_2(CN\text{-}t\text{-}Bu)_4]^{2+}$	6068 [10]	
$[PtRh(dppm)_2(CN)_2(CN\text{-}t\text{-}Bu)_2]^+$	4047	3.043(2)

[a] dpam = bis(diphenylarsino)methane. TMB = 2,5-dimethyl-2,5-diisocyanohexane. [b] Mague, J. T. *Inorg. Chem.* **1969**, *9*, 1975. [c] Simth, D. C.; Miskowski, V. M.; Mason, W. R.; Gray, H. B. *J. Am. Chem. Soc.* **1990**, *112*, 3759.

Figure 3a displays a molecular orbital diagram for *trans*-$[Rh(PMe_3)_2(CN\text{-}t\text{-}Bu)_2]^+$ based on an EHMO calculation (in our calculation, the complex *trans*-$[Rh(PMe_3)_2(CN\text{-}t\text{-}Bu)_2]^+$ rather than *trans*-$[Rh(PPh_3)_2(CN\text{-}t\text{-}Bu)_2]^+$ was used). The order of the d-orbitals of Rh(I) in a square planar geometry should be $d_{x^2-y^2} > d_{z^2} > (d_{xz}, d_{yz}) > d_{xy}$, but in this complex the order is $d_{x^2-y^2} > d_{z^2} > d_{yz} > d_{xy} > d_{xz}$, where the x-direction is along Rh–P and the y-direction is along Rh–CN. The HOMO is a d_{z^2} orbital of Rh, and the LUMO is a combination of p_z on Rh, π^* of CN, and (p_z, d_{xz}) on P. The two intensive absorption bands (397, 317 nm) shown in Figure 2 are assigned to transitions to this LUMO from d_{z^2}(Rh) and d_{yz}(Rh), respectively. From an EHMO calculation, the calculated energy differences for these two transitions are 3.565 and 3.629 eV, respectively. Figure 3b shows a molecular orbital diagram for $[Pt^{II}Rh^{I}(dmpm)_2(CN)_2(CN\text{-}t\text{-}Bu)_2]^+$ (the dppm is replaced by $(CH_3)_2PCH_2P(CH_3)_2$ in the calculation) based on the EHMO calculation. The orbital energies of the d-orbitals of Rh in this complex are roughly the same as that in *trans*-$[Rh(PMe_3)_2(CN\text{-}t\text{-}Bu)_2]^+$. Weak interaction between the

(11) Che, C.-M.; Yam, V. W.-W.; Wong, W.-T.; Lai, T.-F. *Inorg. Chem.* **1989**, *28*, 2908.
(12) Balch, A. L. *J. Am. Chem. Soc.* **1976**, *98*, 8049.
(13) Isci, H.; Mason, W. R. *Inorg. Chem.* **1975**, *14*, 913.
(14) (a) Yersin, H.; Gliemann, G. *Ann. N. Y. Acad. Sci.* **1978**, *313*, 539. (b) Yersin, H.; Gliemann, G.; Rossler, U. *Solid State Commun.* **1977**, *21*, 915.

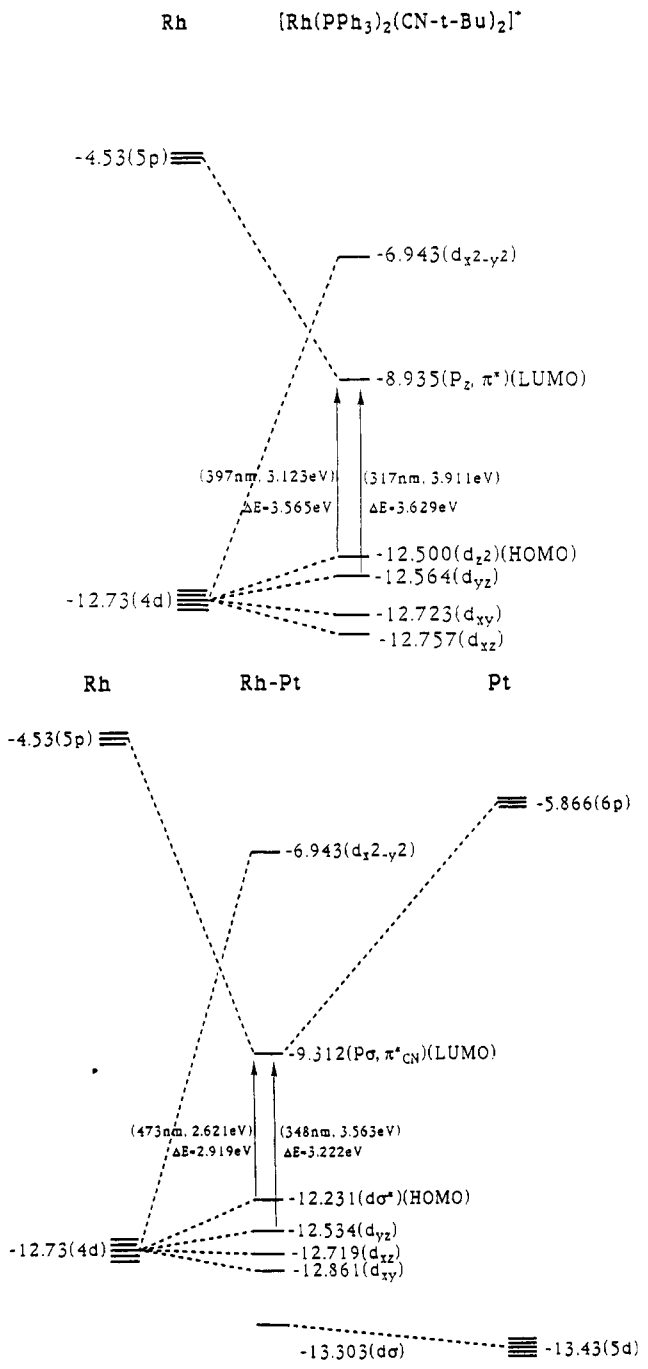

Figure 3. Molecular orbital diagrams of (a, top) *trans*-$[Rh^{I}(PPh_3)_2(CN\text{-}t\text{-}Bu)_2]^+$ and (b, bottom) $[Pt^{II}Rh^{I}(dmpm)_2(CN)_2(CN\text{-}t\text{-}Bu)_2]^+$.

$4d_{z^2}$(Rh) and $5d_{z^2}$(Pt) orbitals gives rise to dσ and dσ* orbitals. The dσ orbital is mainly from the $5d_{z^2}$(Pt), and dσ* is from $4d_{z^2}$-(Rh). The calculation showed that the coefficients of the $4d_{z^2}$ of Rh and $5d_{z^2}$ of Pt in the dσ* (dσ) orbitals are 0.82 (0.38) and 0.45 (0.60), respectively. The destabilization of dσ* is about 0.27 eV from the $4d_{z^2}$ orbital of Rh monomer complex (Figure 3a). A contour diagram showing the wave function of the dσ* orbital is given in Figure 4a. The pσ orbital in Figure 4b mainly comes from $5p_y$(Rh), π* orbitals of isocyanides, and (p_z, d_{xz}) orbitals of phosphorus. The wave function of this orbital shown in Figure 4b is similar to that of the LUMO of *trans*-$[Rh(PMe_3)_2(CN\text{-}t\text{-}Bu)_2]^+$. However, the stabilization of this orbital from the LUMO of the Rh monomer is quite substantial, i.e. 0.38 eV (Figure 3a,b). With these results, it is apparent that the 473-nm band of $[PtRh(dppm)_2(CN)_2(CN\text{-}t\text{-}Bu)_2]^+$, which is assigned to the $^1(d\sigma^* \rightarrow p\sigma)$ transition ($^1A_1 \leftarrow {}^1A_1$, asuming a C_{2v} symmetry

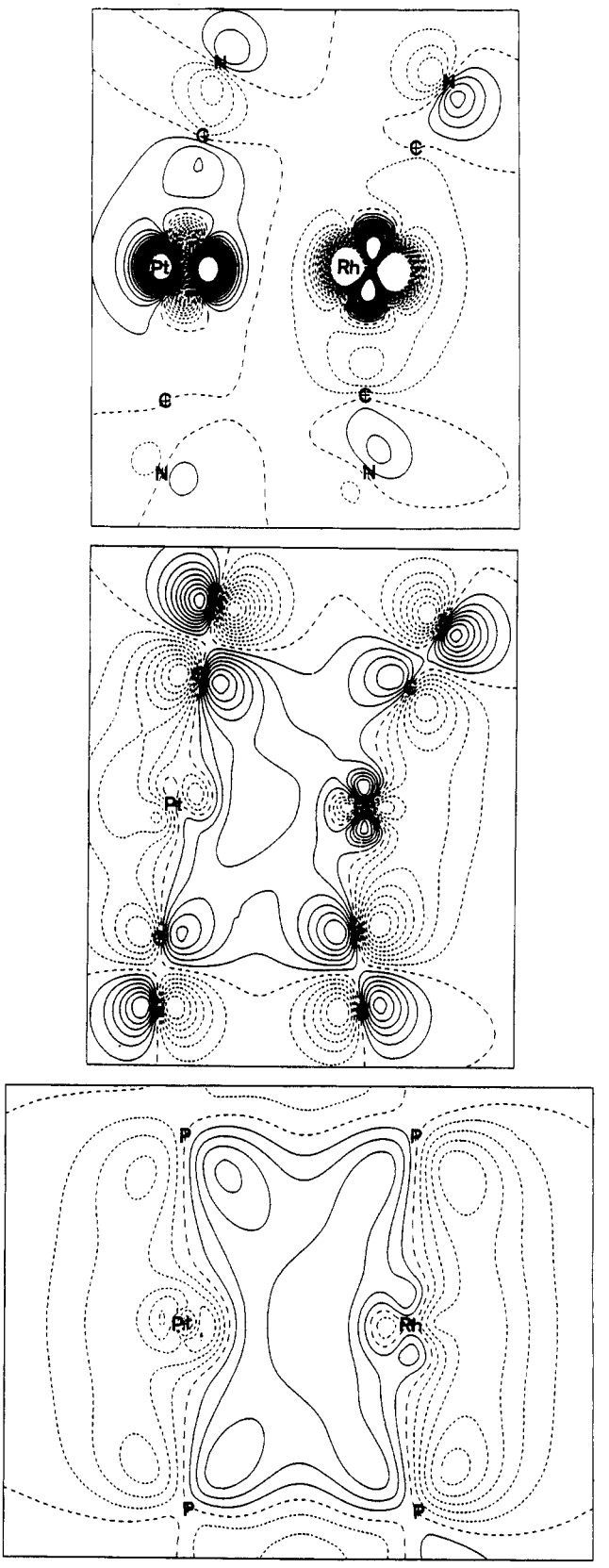

Figure 4. Contour plots of the wave functions of (a, top) dσ* and (b, middle; c, bottom) pσ orbitals and π* of CN^- of $[Pt^{II}Rh^{I}(dmpm)_2(CN)_2(CN\text{-}t\text{-}Bu)_2]^+$.

for the complex), has a significant extent of Rh → π* (isocyanide, phosphine) charge-transfer character.

The transition at 317 nm of *trans*-$[Rh(PPh_3)_2(CN\text{-}t\text{-}Bu)_2]^+$ is red-shifted to 348 nm in $[Pt^{II}Rh^{I}(dppm)_2(CN)_2(CN\text{-}t\text{-}Bu)_2]^+$. The latter absorption band is assigned to the $^1(d_{yz} \rightarrow p\sigma)$ ($^1B_2 \rightarrow {}^1A_1$) transition. The energy difference between the two transitions

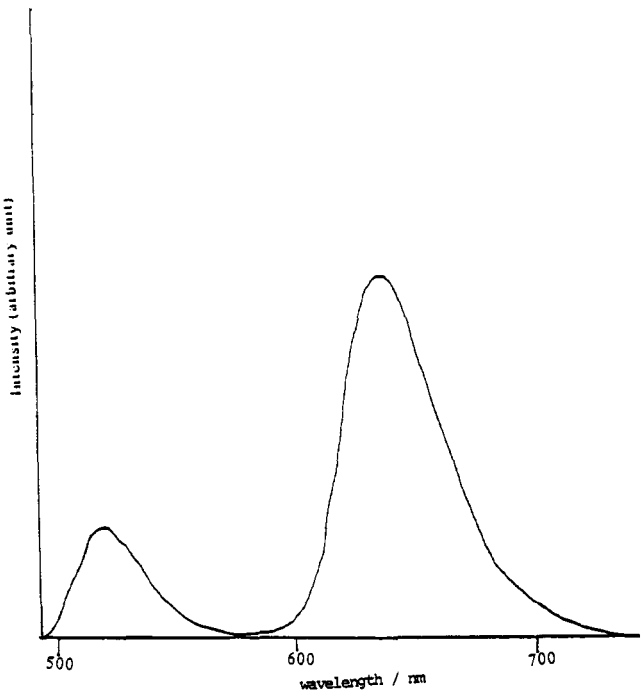

Figure 5. 77 K emission spectrum of $[Pt^{II}Rh^{I}(dppm)_2(CN)_2(CN\text{-}t\text{-}Bu)_2]ClO_4$ measured in an *n*-butyronitrile glass solution.

is only about 2810 cm^{-1} (cf. the calculated difference of 0.30 eV (2420 cm^{-1})). This value is smaller than the energy difference between the $^1(d_{z^2} \rightarrow p_z, \pi^*)$ and $^1(d\sigma^* \rightarrow p\sigma)$ transitions (calculated, 0.65 eV (5243 cm^{-1}); experimental, 4047 cm^{-1}). Such a finding is not unexpected since the interaction between the d_{yz} orbitals is smaller than that between the d_{z^2} orbitals of the two metal ions.

Photoexcitation of a solid sample of $[Pt^{II}Rh^{I}(dppm)_2(CN)_2(CN\text{-}t\text{-}Bu)_2]ClO_4$ at 470 nm results in two emissions centered at 520 and 638 nm. The room-temperature lifetimes of the 520- and 610-nm emissions are <20 ns and 0.1 μs, respectively. On the basis of the lifetimes and Stokes shift of the emission from the lowest energy allowed absorption band, the 520-nm emission is assigned to fluorescence $^1(d\sigma^{*1}p\sigma^1) \rightarrow {}^1(d\sigma^{*2}p\sigma^0)$ ($^1A_1 \rightarrow {}^1A_1$) while the 610-nm one is assigned to phosphorescence $^3(d\sigma^{*1}p\sigma^1) \rightarrow {}^1(d\sigma^{*2}p\sigma^0)$ ($^3A_1 \rightarrow {}^1A_1$). These two emissions become intensified and reduced in width at low temperature. Figure 5 shows the 77 K emission spectrum measured in an *n*-butyronitrile glass solution. The maxima of the two emission bands change to 521 and 637 nm at 77 K. The singlet ($^1A_1$) and triplet ($^3A_1$) splitting, measured from the fluorescence and phosphorescence maxima, is 3495 cm^{-1}. This value is very close to the 3500-cm^{-1} splitting found in a number of Rh(I) monomers with chelating diphosphine ligands.[15]

The excitation spectrum of the emission shows two bands centered at 351 and 483 nm, which correspond to the $^1(d_{yz} \rightarrow p\sigma)$ and $^1(d\sigma^* \rightarrow p\sigma)$ transitions, respectively. A shoulder at 367 nm is observed in the 351-nm excitation band.

The mononuclear *trans*-$[Rh^{I}(PPh_3)_2(CN\text{-}t\text{-}Bu)_2]^+$ displays emission at low temperature. Figure 6 shows its 77 K emission spectrum measured in an *n*-butyronitrile glass solution. The 580-nm emission is assigned to the $^3(p_z, \pi^* \rightarrow d_{z^2})$ phosphorescence. The excitation spectrum of this emission consists of bands at 319, 347, 398, and 468 nm. The last two excitation bands are $^1(d_{z^2} \rightarrow p_z, \pi^*)$ and $^3(d_{z^2} \rightarrow p_z, \pi^*)$ transitions, respectively. It is found that the difference in phosphorescent energy between *trans*-$[Rh^{I}(PPh_3)_2(CN\text{-}t\text{-}Bu)_2]^+$ and $[PtRh(dppm)_2(CN)_2(CN\text{-}t\text{-}Bu)_2]^+$ (1540 cm^{-1}) is smaller than the corresponding difference in $^1(d_{z^2} \rightarrow p_z, \pi^*)$ and $^1(d\sigma^* \rightarrow p\sigma)$ absorptions (4047 cm^{-1}). In other words, the Stoke shift of emission of $[PtRh(dppm)_2(CN)_2(CN\text{-}t\text{-}Bu)_2]^+$ is smaller than that of *trans*-$[Rh(PPh_3)_2(CN\text{-}t\text{-}Bu)_2]^+$. This would mean a smaller excited-state distortion of the dinuclear complex than the Rh monomer.

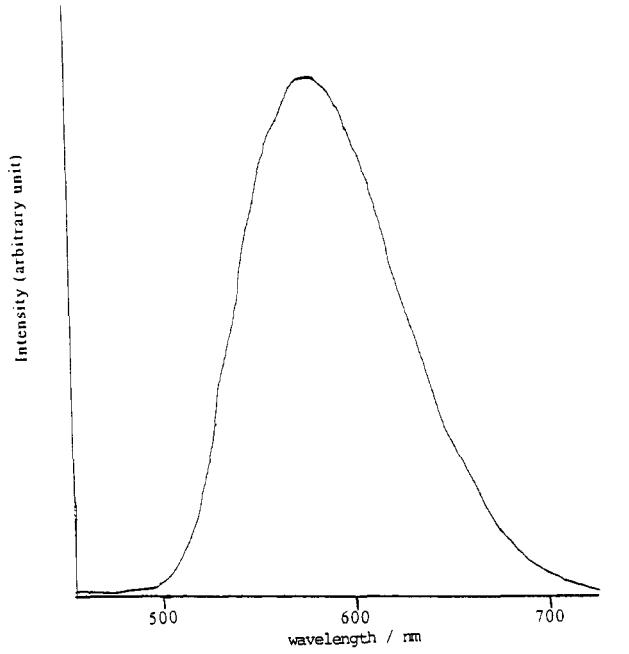

Figure 6. 77 K emission spectrum of *trans*-$[Rh^{I}(PPh_3)_2(CN\text{-}t\text{-}Bu)_2]ClO_4$ measured in an *n*-butyronitrile glass solution.

Heterobimetallic d^{10}–d^8 Complexes. There are only few examples of luminescent heterobimetallic d^{10}–d^8 complexes, including $[IrAu(dppm)_2(CO)Cl]^+$ studied by Balch *et al.*[1f] and $[MPt(dppm)_2(CN)_2]^+$ [1g] and $[MPt(dppm)_2(C{\equiv}CPh)_2]^+$ (M = Au^+, Ag^+) studied by Che and co-workers.[1e,16] In order to further our understanding of the interaction between d^8 and d^{10} metal ions, we have investigated the spectroscopic properties of $[MRh(dppm)_2(CN\text{-}t\text{-}Bu)_2]^{2+}$ (M = Au^+, Ag^+), which were first synthesized by Shaw and co-workers.[5b]

Analogous to the heterobimetallic complexes $[PtRh(dppm)_2(CN)_2(CN\text{-}t\text{-}Bu)_2]^+$ and $[AuPt(dppm)_2(CN)_2]^+$, for $[MRh(dppm)_2(CN\text{-}t\text{-}Bu)_2]^{2+}$, the antibonding interaction between the d_{z^2} orbitals of Rh and M would give rise to $d\sigma^*$, while the bonding interaction of the p_z orbitals leads to $p\sigma$. Figure 7 gives a qualitative molecular orbital diagram of $[MRh(dppm)_2(CN\text{-}t\text{-}Bu)_2]^{2+}$.

The absorption spectra of $[AuRh(dppm)_2(CN\text{-}t\text{-}Bu)_2](ClO_4)_2$ and $[AgRh(dppm)_2(CN\text{-}t\text{-}Bu)_2](ClO_4)_2$ measured at room temperature are shown in Figure 8. Both spectra exhibit two intense absorption bands in the visible region with λ_{max} ($\epsilon_{max}/M^{-1}\ cm^{-1}$) at 342 ($9.44 \times 10^3$) and 455 ($2.4 \times 10^4$) for $[AuRh(dppm)_2(CN\text{-}t\text{-}Bu)_2](ClO_4)_2$ and 330 nm (1.19×10^4) and 425 nm (1.68×10^4) for $[AgRh(dppm)_2(CN\text{-}t\text{-}Bu)_2](ClO_4)_2$. The 455-nm band of the former and 420-nm band of the latter are both assigned to the $^1(d\sigma^* \rightarrow p\sigma)$ transition as in the d^8–d^8 systems (see Figure 6). The 342- and 327-nm absorption bands are tentatively assigned to the $^1(d_{yz}(Rh) \rightarrow p\sigma)$ transitions of the complexes, analogous to the 348-nm band of $[PtRh(dppm)_2(CN)_2(CN\text{-}t\text{-}Bu)_2]^+$. The spectrum of $[AuRh(dppm)_2(CN\text{-}t\text{-}Bu)_2](ClO_4)_2$ also shows a weak absorption at 525 nm ($\epsilon \approx 6 \times 10^2\ M^{-1}\ cm^{-1}$), which is assigned to the $^3(d\sigma^* \rightarrow p\sigma)$ transition. Table II compares the $^1(d\sigma^* \rightarrow p\sigma)$ transitions of $[PtRh(dppm)_2(CN)_2(CN\text{-}t\text{-}Bu)_2]^+$, $[AuRh(dppm)_2(CN\text{-}t\text{-}Bu)_2]^{2+}$, and $[AgRh(dppm)_2(CN\text{-}t\text{-}Bu)_2]^{2+}$ with the $^1(d_{z^2} \rightarrow p_z, \pi^*)$ transition of *trans*-$[Rh(PPh_3)_2(CN\text{-}t\text{-}Bu)_2]^+$. The energy differences of the transitions between the dinuclear complexes and Rh(I) monomer are in the order Pt-

(15) Geoffroy, G. L.; Wrighton, M. S.; Hammond, G. S.; Gray, H. B. *J. Am. Chem. Soc.* **1974**, *96*, 3105.

(16) Yip, H.-K.; Lin, H.-M.; Wang, Y.; Che, C.-M. Submitted for publication.

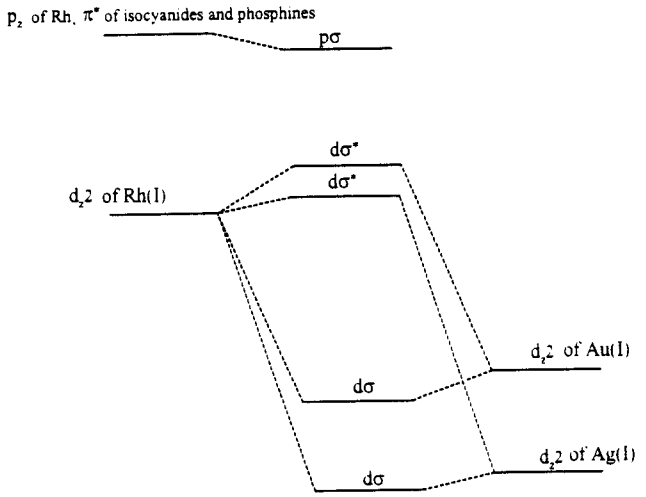

Figure 7. Molecular orbital diagram for $[MRh(dppm)_2(CN\text{-}t\text{-}Bu)_2]^{2+}$ ($M = Au^+, Ag^+$).

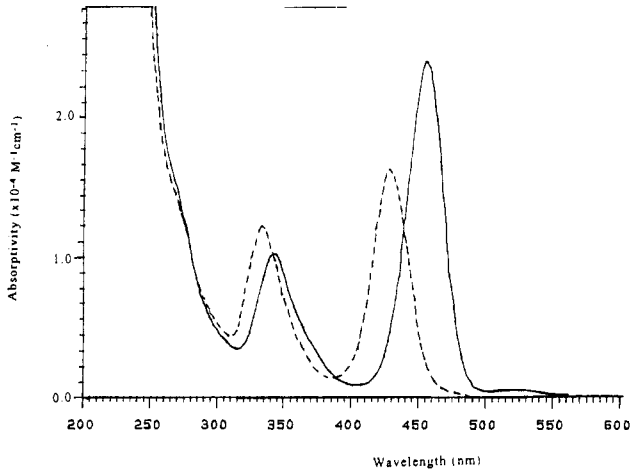

Figure 8. Room-temperature absorption spectra of acetonitrile solutions of $[AuRh(dppm)_2(CN\text{-}t\text{-}Bu)_2](ClO_4)_2$ (—) and $[AgRh(dppm)_2(CN\text{-}t\text{-}Bu)_2](ClO_4)_2$ (- - -).

Table II. Energy Differences between $^1(d\sigma^* \rightarrow p\sigma)$ Transitions of the Dinuclear Complexes and the $^1(d_{z^2} \rightarrow p_z)$ Transition (25 188 cm^{-1}) of *trans*-$[Rh(PPh_3)_2(CN\text{-}t\text{-}Bu)_2]^+$

complex	energy diff (cm^{-1})
$[PtRh(dppm)_2(CN)_2(CN\text{-}t\text{-}Bu)_2]^+$	4047
$[AuRh(dppm)_2(CN\text{-}t\text{-}Bu)_2]^{2+}$	3210
$[AgRh(dppm)_2(CN\text{-}t\text{-}Bu)_2]^{2+}$	1659

(II)–Rh(I) > Au(I)–Rh(I) > Ag(I)–Rh(I). This suggests that the extent of metal–metal interaction of the complexes may follow a similar order. The extent of orbital interaction is dependent on the orbital overlap and energy difference between the interacting orbitals. The spectroscopic result is, therefore, in accordance with the fact that the d-orbital energies of the metal ions are in the order Rh(I) > Pt(II) > Au(I) > Ag(I).

The two heterobimetallic d^{10}–d^8 complexes also show intriguing luminescent properties. Figure 9 shows the emission spectra of $[AuRh(dppm)_2(CN\text{-}t\text{-}Bu)_2](ClO_4)_2$ (excitation wavelength = 450 nm) measured in the solid form at room temperature and in a 77 K glass solution. While the solid exhibits a structureless emission at 610 nm (lifetime = 0.5 μs), two emission bands centered at 500 and 610 nm are found in the glassy solution. The two emissions are tentatively assigned to the fluorescence and phosphorescence derived from the $^1(d\sigma^*p\sigma)$ and $^3(d\sigma^*p\sigma)$ states, respectively. The excitation spectrum of the 77 K *n*-butyronitrile glass emission is composed of four bands centered at 339, 373, 466, and 546 nm. The last two excitation bands are assigned to the $^1(d\sigma^* \rightarrow p\sigma)$ and $^3(d\sigma^* \rightarrow p\sigma)$ transitions, respectively. Both

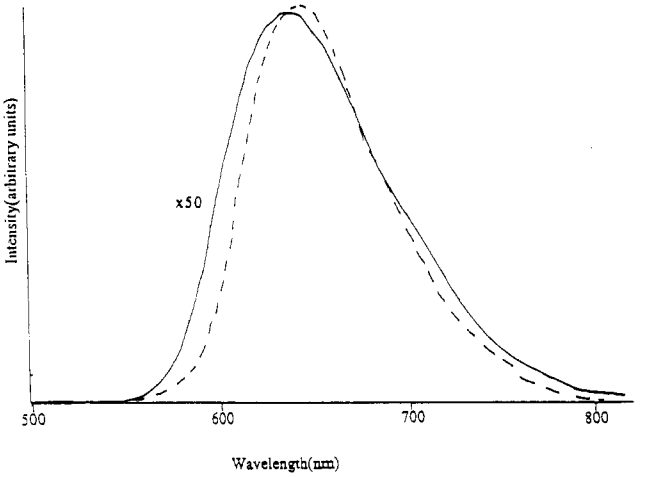

Figure 9. Room-temperature (solid state, —) and 77 K (*n*-butyronitrile glass (- - -) emission spectra of $[AuRh(dppm)_2(CN\text{-}t\text{-}Bu)_2](ClO_4)_2$.

$^1(d\sigma^* \rightarrow p\sigma)$ and $^3(d\sigma^* \rightarrow p\sigma)$ transitions recorded in the 77 K excitation spectrum are red-shifted from that recorded in the room-temperature absorption spectrum (see Figure 8), and this is not unreasonable since both transitions are expected to be accompanied by an increase of Au–Rh bond order.

The separation between the singlet and triplet of $(d\sigma^* \rightarrow p\sigma)$ transitions, measured from the 77 K excitation spectrum, is about 3140 cm^{-1}. The value of splitting is comparable to the analogous singlet–triplet separation found in the MLCT transition of the monomeric *trans*-$[Rh(PPh_3)_2(CN\text{-}t\text{-}Bu)_2]^+$ (3760 cm^{-1}), suggesting that in $[AuRh(dppm)_2(CN)_2(CN\text{-}t\text{-}Bu)_2]^{2+}$ the $^1(d\sigma^* \rightarrow p\sigma)$ transition can be viewed to be mainly derived from the Rh $\rightarrow \pi^*$(isocyanide, phosphine) transition.

$[AgRh(dppm)_2(CN\text{-}t\text{-}Bu)_2](ClO_4)_2$ is found to be a weakly emissive solid at room temperature. The solid-state emission at 575 nm (lifetime ~ 0.05 μs at room temperature) is slightly red-shifted to 583 nm in a 77 K *n*-butyronitrile glass solution. It is noted that the $^1(d\sigma^* \rightarrow p\sigma)$ transition and $^3(d\sigma^*p\sigma)$ emission of $[AgRh(dppm)_2(CN\text{-}t\text{-}Bu)_2]^{2+}$ are both very close to the $^1(d_{z^2} \rightarrow \pi^*, p_z)$ transition and $^3(d_{z^2}p_z)$ emission of *trans*-$[Rh(PPh_3)_2(CN\text{-}t\text{-}Bu)_2]$. Thus, $[AgRh(dppm)_2(CN\text{-}t\text{-}Bu)_2]^{2+}$ can be considered to be an extreme case of dinuclear complex, in which the perturbation of one metal on the other is small. The excitation spectrum exhibits bands at 331, 361, and 439 nm. The 439-nm excitation band is due to the $^1(d\sigma^* \rightarrow p\sigma)$ transition.

Balch and co-workers have reported the absorption and emission spectra of a d^{10}–d^8 complex, $[AuIr(dppm)_2(CO)Cl]^+$. The $^1(d\sigma^* \rightarrow p\sigma)$ transition of the complex is located at 440 nm, while the $^1(5d_{z^2} \leftarrow 6p_z, \pi^*)$ transition of the mononuclear *trans*-$[Ir(PPh_3)_2(CO)Cl]$ has λ_{max} located at 387 nm. The energy difference of 3112 cm^{-1} between the two transitions is quite significant, suggesting the orbitals of the Ir and Au ions are not well matched and the $d\sigma^*$ orbital is predominantly contributed from the $5d_{z^2}$(Ir) orbital. From the spectroscopic study on $[PtRh(dppm)_2(CN)_2(CN\text{-}t\text{-}Bu)_2]^+$ and $[MRh(dppm)_2(CN\text{-}t\text{-}Bu)_2]^+$ ($M = Au^+, Ag^+$), it is reasonable to expect the $^1(d\sigma^* \rightarrow p\sigma)$ transition of $[AuIr(dppm)_2(CO)Cl]^+$ may contain to a certain extent the charge-transfer character of the Ir moiety.

Conclusion

In this work, the spectroscopic properties of several new luminescent heterobimetallic complexes are described. Although the metal–metal interaction of homodinuclear d^8 metal complexes is well understood, the interaction between two metal ions with

different electronegativities still remains to be explored. The present study suggests that electronic spectroscopy is a useful tool to study this kind of metal–metal interaction. It is reasonable to expect that by judicious choice of auxiliary ligand, heterobimetallic Pt(II)–Rh(I) complexes with long-lived electronic excited states could be synthesized and may be expected to display intriguing photochemical reactions.

Acknowledgment. We acknowledge support from the Croucher Foundation, the Research Grants Council of Hong Kong, and the National Science Council (NSC) of Taiwan. C.-M.C. is thankful for a visiting professorship administered by the National Taiwan University. H.-K.Y. is thankful for a Croucher Studentship, administered by the Croucher Foundation of Hong Kong.